https://doi.org/10.1093/plphys/kiac430 PLANT PHYSIOLOGY 2022: 190: 2187–2202

Plant Physiology®

Research Article

Clay nanoparticles efficiently deliver small interfering RNA to intact plant leaf cells

Jiaxi Yong [1], Miaomiao Wu [1], Run Zhang [1], Shengnan Bi [2], Christopher W. G. Mann,[2] Neena Mitter [3], Bernard J. Carroll [2,*] and Zhi Ping Xu [1,*]

1 Australian Institute for Bioengineering and Nanotechnology, The University of Queensland, Brisbane, QLD 4072, Australia
2 School of Chemistry and Molecular Biosciences, The University of Queensland, Brisbane, QLD 4072, Australia
3 Queensland Alliance for Agriculture and Food Innovation, The University of Queensland, Brisbane, QLD 4072, Australia

*Authors for correspondence: gordonxu@uq.edu.au (Z.P.X.), b.carroll@uq.edu.au (B.C.).

J. Y., B.C. R.Z., and Z.P.X. conceptualized and designed the research. J.Y. conducted experiments, data analysis, and wrote the first draft. M.W conducted experiments, data analysis, and conceptual visualization. S.B. and C.M. conducted the experiments. J.Y., R.Z., B.C., N.M., and Z.P.X. wrote and revised the manuscript. All authors read and commented on the manuscript.

The author responsible for distribution of materials integral to the findings presented in this article in accordance with the policy described in the Instructions for Authors (https://academic.oup.com/plphys/pages/general-instructions) is Zhi Ping Xu (gordonxu@uq.edu.au).

Abstract

RNA interference is triggered in plants by the exogenous application of double-stranded RNA or small interfering RNA (siRNA) to silence the expression of target genes. This approach can potentially provide insights into metabolic pathways and gene function and afford plant protection against viruses and other plant pathogens. However, the effective delivery of biomolecules such as siRNA into plant cells is difficult because of the unique barrier imposed by the plant cell wall. Here, we demonstrate that 40-nm layered double hydroxide (LDH) nanoparticles are rapidly taken up by intact *Nicotiana benthamiana* leaf cells and by chloroplasts, following their application via infiltration. We also describe the distribution of infiltrated LDH nanoparticles in leaves and demonstrate their translocation through the apoplast and vasculature system. Furthermore, we show that 40-nm LDH nanoparticles can greatly enhance the internalization of nucleic acids by *N. benthamiana* leaf cells to facilitate siRNA-mediated downregulation of targeted transgene mRNA by $>70\%$ within 1 day of exogenous application. Together, our results show that 40-nm LDH nanoparticle is an effective platform for delivery of siRNA into intact plant leaf cells.

Introduction

Recent developments in biotechnology have enabled effective molecular manipulation of plant physiology by topical application of exogenous biomolecules, including DNA, RNA, and proteins, for plant science research, and enhanced agricultural and pharmaceutical production (Koch and Kogel, 2014; Altpeter et al., 2016; Lv et al., 2020). In particular, RNA interference (RNAi) induced by topical application of double-stranded RNA (dsRNA) or small interfering RNA (siRNA) has been demonstrated to be an effective technology for plant protection against viruses and other invading pathogens, as well as to provide an alternate platform to molecularly manipulate metabolic and synthetic pathways in planta (Key et al., 2008; Koch and Kogel, 2014; Guo et al., 2019; Liu et al., 2021). However, the cell wall and plasma membrane of plant cells limit the internalization of topically delivered biomolecules (Bennett et al., 2020). Therefore, various approaches have long been sought to deliver biomolecules into intact plant cells. These methods include the use of *Agrobacterium tumefaciens*-based, viral-based transformation systems, and biolistic gene guns, and direct leaf spray specifically for the delivery of dsRNA or siRNA. Given that (1) Agrobacterium and viral transformation systems are species dependent and restricted to the transfer of DNA, (2)

Received May 04, 2022. Accepted August 16, 2022. Advance access publication September 22, 2022

Open Access

damages often occur to the plant tissues, cells, and genome after biolistic bombardment, (3) the biomolecule cargos are fragile and easily denatured, and (4) effective delivery of biomolecules to subcellular structures may be required, there is a need for more feasible, benign, biocompatible, and universal delivery approaches (Cunningham et al., 2018; Liu et al., 2019; Wang et al., 2019; Torti et al., 2021; Hoang et al., 2022; Uslu et al., 2022).

Nanoparticles have been demonstrated to be efficient vehicles for the delivery of biomolecules and/or pharmaceutics into mammalian cells (Cao et al., 2020; Sun et al., 2021). Recently, nanoparticles have also been investigated as carriers for biomolecule delivery into intact plant tissues. For example, layered double hydroxides (LDHs), carbon-based nanomaterials, mesoporous silica nanoparticles, DNA nanostructures, and gold clusters, have all been used for the successful delivery of plasmid DNA or RNA into intact plant tissues to modify gene expression, edit the plant genome, and/or manipulate plant cell physiology (Martin-Ortigosa et al., 2014; Mitter et al., 2017; Demirer et al., 2019; Hua et al., 2019; Zhang et al., 2019; Schwartz et al., 2020; Zhang et al., 2021). When compared to conventional approaches, nanoparticle-mediated delivery of biomolecules into plant cells offers several advantages, including species independence, almost no damage to plant tissues and genomes, the controlled release of delivered biomolecular cargo, and the capacity to target-specific subcellular structures (Mitter et al., 2017; Kwak et al., 2019; Santana et al., 2020). Indeed, nanoparticles have the potential to enable the delivery of biomolecules into plant cells and cellular compartments in a noninvasive way.

LDH is a family of biocompatible and degradable hydrotalcite-like clay materials with mixed divalent and trivalent metal hydroxide layers, between which there are intercalated anions and water molecules (Xu and Zeng, 2001). The distinct layer structure and positively charged nature enable LDH nanoparticles to be suitable biomolecule carriers, along with good biocompatibility, which has been effectively demonstrated in biomedical and pharmaceutical applications (Xu et al., 2006b; Chen et al., 2018b). LDH nanomaterials have also been shown to effectively protect plants against viruses via their slow release of anti-virus dsRNA onto the leaf surface (Mitter et al., 2017). Furthermore, small LDH nanoparticles (<50 nm) have been demonstrated to enhance dsRNA internalization by developing pollen to induce efficient RNAi (Yong et al., 2021). However, it remains to be understood whether intact leaf cells can take up LDH nanoparticles along with biomolecules, or nanocarriers can translocate within the leaf and plant. Addressing these questions will provide further mechanistic insight into the possibility of designing new nanoparticle platforms for efficient delivery of biomolecules into whole plants.

Hence, the aim of this research was to: (1) elucidate whether 40-nm LDH nanoparticles infiltrated into the leaf are internalized by intact leaf cells; (2) investigate whether LDH nanoparticles are translocated in the leaf apoplast and/or the vasculature system; and (3) use LDH nanoparticles to deliver siRNA molecules into intact leaves to efficiently induce silencing of a target gene. We demonstrate that 40-nm LDH nanoparticles translocate within the apoplast regions and the vasculature system of leaves, and are subsequently internalized into plant cells and chloroplasts, and facilitate the delivery of siRNA for effective target gene silencing. Taken together, the findings reported in this study show that small LDH nanoparticles form an efficient and alternate platform for the delivery of exogenous biomolecules into intact leaves, with chloroplast penetrating ability, for plant trait modification.

Results

Characteristics of LDH nanoparticles

The hexagonal sheet-like morphology of well dispersed LDH nanoparticles can be clearly observed via transmission electron microscopy (TEM) imaging (Figure 1A). The sheet diameter of LDH nanoparticles measured in these TEM images was distributed in the range of 20–70 nm, with the majority of nanoparticles having the diameter of 30–50 nm and an average diameter of ~41 nm (Figure 1B). This distribution was in accordance strongly with the particle size distribution measured by dynamic light scattering (DLS; Figure 1B; Supplemental Table S1), with the average hydrodynamic diameter of 34 nm and a ζ-potential of 43 mV. As illustrated in Supplemental Figure S1 and Supplemental Table S1, labeling with FITC did not change the characteristics of the LDH nanoparticles, while loading of the siRNA cargo caused a slight degree of particle aggregation and slightly increased the average diameter to 45 nm (Supplemental Table S1). The atomic force microscopy image (Figure 1C) showed the majority of LDH nanoparticles had the thickness in the range of 4–8 nm, with an average thickness of around 5.8 nm (Supplemental Table S1) as well as an average diameter of 38 nm, which is in accordance with the TEM-based estimation (41 nm). Thus, the ratio of the average diameter to the estimated thickness of these LDH nanoparticles was approximately 6–7, a reflection of the platelet-like nature of LDH nanoparticles (Xu et al., 2007). The X-ray diffraction (XRD) pattern (Figure 1D) showed characteristic diffraction peaks typical of LDH nanoparticles (Xu and Zeng, 2001), with 2θ angles at 11.5°, 23.0°, and 34.6° corresponding to (003), (006), and (012) crystal planes, respectively.

Foliar uptake of LDH nanoparticles through leaf infiltration

Fluorescein isocyanate-labeled LDH nanoparticles (LDH–FITC) were infiltrated into wild-type *Nicotiana benthamiana* leaves through the abaxial surface of the leaf with a needleless syringe to assess the degree of internalization of the LDH–FITC nanoparticles by leaf cells. The abaxial epidermal layer and spongy mesophyll cells of infiltrated leaves (Figure 2, A and B) were imaged with a confocal imaging system at 90 min after infiltration. The magenta autofluorescence of chlorophyll was adopted as the indicator to identify

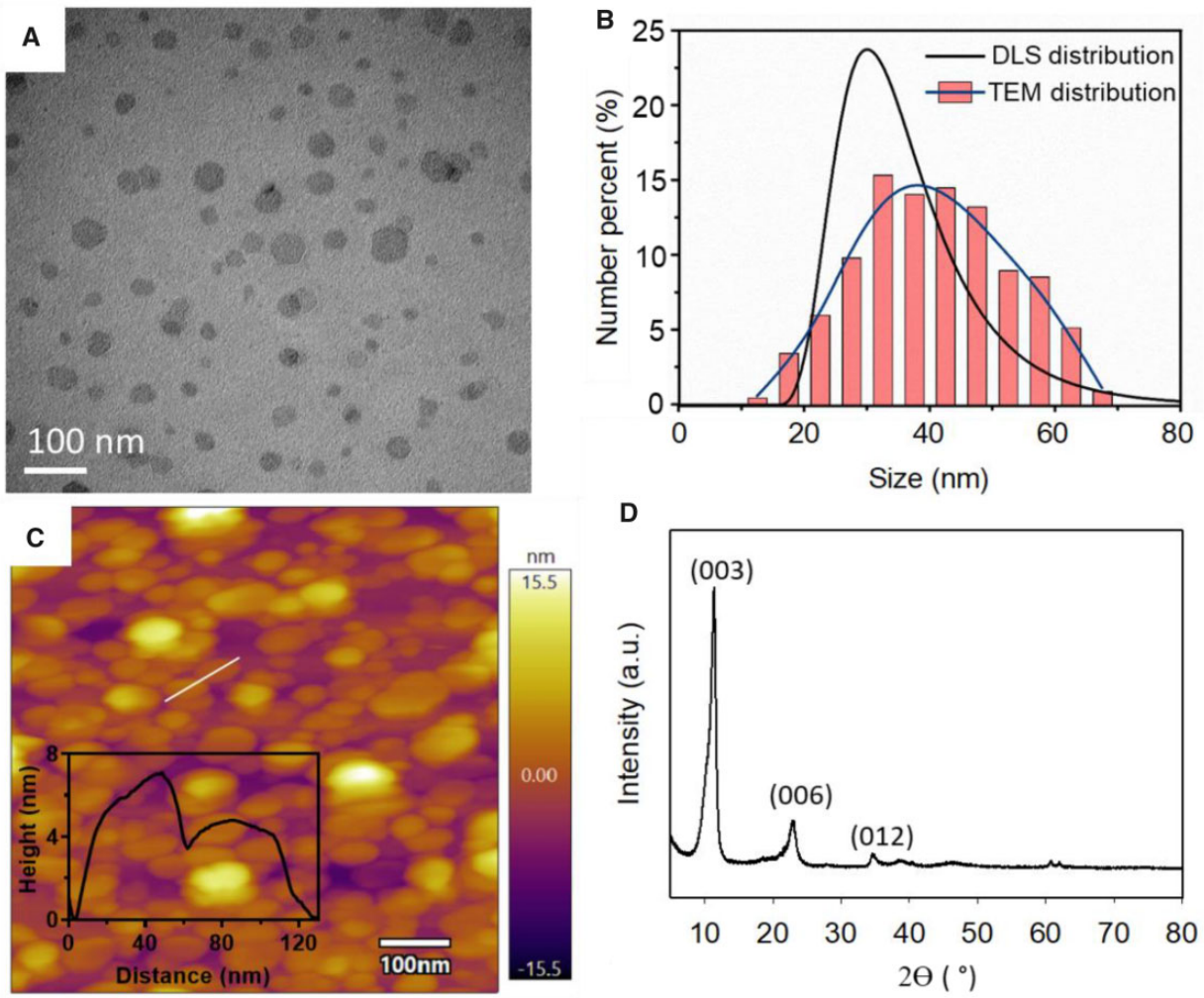

Figure 1 Physicochemical characteristics of LDH nanoparticles investigated in this study. A, Representative TEM image of LDH nanoparticles (bar, 100 nm). B, Size distribution of LDH nanoparticle measured by dynamic light scattering (DLS) and counted from TEM images (bars and simulated line). C, Representative atomic force microscope (AFM) image of LDH nanoparticles and representative thickness curve of LDH nanoparticles (insert graph). D, XRD pattern of LDH nanoparticles, with characteristic crystal plane indexes corresponding to the peaks.

the intracellular region of mesophyll and epidermal cells. As expected, infiltration of free FITC dye showed negligible green fluorescence (Figure 2A). However, in leaves infiltrated with an equivalent concentration of FITC delivered in complex with LDH nanoparticles, termed LDH–FITC (i.e. 100 μL of LDH–FITC, 10 mg · L^{-1} of FTIC loaded with 200 mg·L^{-1} of LDH–FITC), a very strong and consistent green florescent signal was observed within mesophyll cells at 90-min post infiltration (Figure 2A).

Very strong green fluorescence was found with or around the magenta chloroplast fluorescence of mesophyll cells (Figure 2A), suggesting LDH nanoparticles were not only successfully internalized into the cytosol of these cells. Three-dimensional Z-stack images and the cross-sectional views of infiltrated leaves (Supplemental Figure S2) further illustrated the distribution of LDH–FITC nanoparticles in the leaf cells, where the majority of LDH–FITC nanoparticles were localized to the cytosol of chlorophyll cells at 90-min post infiltration. In addition, clear green fluorescence in the abaxial epidermis and particularly guard cells of LDH–FITC-infiltrated leaves was observed to predominantly localize to the cytosol (Figure 2A; Supplemental Figure S2).

Remarkably, the fluorescence of LDH–FITC nanoparticles in plant cells was confirmed to colocalize with chlorophyll autofluorescence (Figure 2, A and B). Representative quantitative analysis of fluorescence intensity in several individual chloroplasts labeled with white lines #1–5 in Figure 2B demonstrated clear colocalization between the chloroplast channel and the LDH–FITC channel (Figure 2C). Since chlorophyll is mainly located on the thylakoid membrane in chloroplasts and the LDH–FITC distribution was slightly deviated from the chlorophyll distribution in high resolution images and intensity analysis, Figure 2, B and C suggest that the nanoparticles are more likely to locate in the stroma of the chloroplasts, instead of the membrane structures. A one-to-one pixel matching colocalization analysis was conducted (Supplemental Figure S3), which showed that the correlation coefficient between the chloroplast and

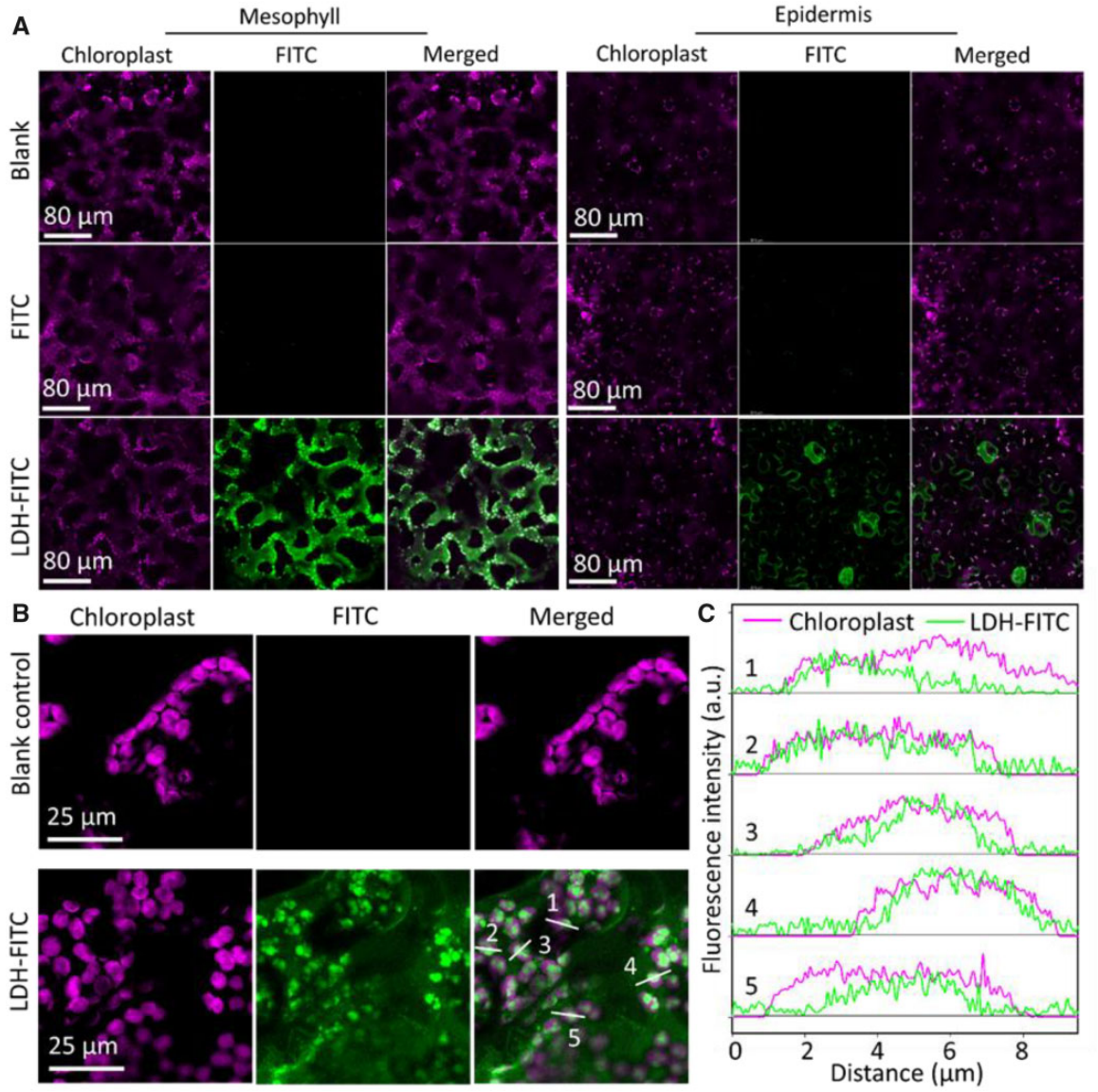

Figure 2 Representative confocal images of LDH internalization by *N. benthamiana* leaves infiltrated via the abaxial surface. A, Confocal images of abaxial mesophyll cells and epidermal cells of nontreated leaves and leaves infiltrated with fluorescein isocyanate (FITC, 10 mg L^{-1}, 100 μL) and FITC-labeled LDH (LDH–FITC, 200 mg L^{-1} LDH, 10 mg L^{-1} FITC, 100 μL) at 90-min post-infiltration. B, High-resolution confocal images of mesophyll cells on the abaxial side of nontreated leaves and leaves infiltrated with LDH–FITC at 90-min post-infiltration. C, Typical fluorescence intensity curves for localization of LDH–FITC and chloroplasts labeled with white lines and 1–5 in (B).

LDH–FITC channels in mesophyll cells was 0.60 ± 0.03 (n = 3), significantly higher than that of the blank control group (0.10 ± 0.01) and FITC alone group (0.16 ± 0.03). The data thus not only reveal the rapid internalization of LDH–FITC nanoparticles into the plant cell cytosol, but also demonstrate the preferential association of the internalized LDH–FITC nanoparticles with chloroplasts. The preferential association was further illustrated by the colocalization of LDH–FITC nanoparticles with isolated chloroplasts upon co-incubation in vitro (Supplemental Figure S4). Taken together, these data infer that the LDH nanoparticles adhere well to the surface of chloroplasts, enabling their subsequent import into the organelles.

We also tested the leaf internalization of LDH–FITC nanoparticles by wheat (*Triticum aestivum*) as a model monocot plant (Supplemental Figure S5). Green fluorescence of LDH–FITC was observed in the cytosol of wheat mesophyll cells at 90-min post infiltration. Similarly, the fluorescence was located around or directly overlaid with the chlorophyll autofluorescence, implying the potential species-independent delivery ability of LDH nanoparticles.

LDH nanoparticles also showed good biocompatibility. As shown in Supplemental Figure S6, negligible damage to plant cells and chloroplasts was observed at 1- or 24-h post leave infiltration with LDH nanoparticles at the doses of 200 and 5,000 mg·L^{-1}, comparable to nontreated leaves.

Meanwhile, a repeated infiltration of LDH nanoparticles at 0 and 48 h and observation at 72 h did not show any damage to the leaves. In contrast, obvious distortion in the leaf cell and chloroplast structure and morphology was observed for leaves at 1 h after infiltration of a positive control for cell damage, namely 2-(N-morpholino)ethanesulfonic acid (MES) buffer containing 1% (w/v) sodium dodecyl sulfate (SDS) (Supplemental Figure S6).

Translocation of LDH nanoparticles in leaves

To further uncover the mechanics of LDH nanoparticle uptake by the cells of infiltrated leaves, we examined the translocation of infiltrated LDH–FITC nanoparticles in the leaves at 30- and 90-min post infiltration. As illustrated in Figure 3A, at 30-min post infiltration, weak green fluorescence emitted from the LDH–FITC nanoparticles was observed in the plant cells of infiltrated leaves. Clearly, the green fluorescence signal did not colocalize with the magenta fluorescence signal of the chloroplasts at this timepoint. This finding indicated that at 30-min post infiltration the majority of LDH–FITC nanoparticles were located within the extracellular space of infiltrated leaves. In sharp contrast, at 90-min post infiltration, a strong green fluorescence signal was evident in the mesophyll cells, and further this signal was observed to primarily colocalize with the magenta fluorescence signal emitted by chloroplasts (Figure 3A). This finding demonstrated that LDH nanoparticles enter the cytosol of leaf mesophyll cells from the extracellular apoplast within 30–90 min of infiltration (Supplemental Figure S7). Furthermore, this observation is highly similar to our previous report that LDH nanoparticles are quickly taken up by developing tomato pollen (Yong et al., 2021). LDH–FITC nanoparticles were also observed within adaxial epidermal and mesophyll cells at 90-min post infiltration (Supplemental Figure S8).

As shown in Figure 3B, when LDH nanoparticles were infiltrated into leaves, they did not show an even pattern of distribution throughout the infiltrated area. At 5 min after infiltration, the accumulation of LDH nanoparticles was highly concentrated around the point of infiltration, and then steadily decreased in intensity according to the distance from the point of infiltration (green line, Figure 3C). Thus, the apoplast seemed to act as a filter to restrict the movement of the LDH nanoparticles relative to the water component of infiltration solution. More specifically, the highest abundance of LDH nanoparticles was located within 0.1–0.3 cm of the infiltration point, whereas the water component of infiltration solution was observed to extend to 1.5–2.5 cm from the point of infiltration. Accordingly, the abundance of LDHs within the infiltrated area of the leaf gradually decreased from approximately 180–190 fluorescence units at the infiltration point, to approximately 12–14 fluorescence units at a distance of 1.4–1.5 cm away from the infiltration point, a value that was nevertheless substantially higher than that of the background signal (<5 units, blue line, Figure 3C). At 90-min post infiltration, the LDH nanoparticle distribution curve had flattened, when compared to the shape of the curve at 5-min post infiltration. A lower fluorescence intensity was observed within 0–0.3 cm of the infiltration point but increased fluorescence was evident at more than 0.3 cm away from the infiltration point (red curve, Figure 3C). The flattening of the distribution curve thus strongly suggests that LDH nanoparticles gradually diffuse from the point of infiltration to the surrounding area within 90 min of their application.

We conducted additional experiments using nanoparticles that were either larger in size (>100 nm), or very small in physical size (3–5 nm), compared to the preferred size of 40 nm for LDH nanosheets. More specifically, larger LDH nanoparticles with an approximate diameter of >100 nm were observed to solely accumulate in the area immediately adjacent to the infiltration point (Supplemental Figure S9). In direct contrast, smaller sized quantum dot nanoparticles of 3–5 nm in diameter were observed to be uniformly distributed throughout the infiltrated area of the leaf immediately post the application of the infiltrate. These images clearly show that the degree of nanoparticle movement through the apoplast was size dependent. Time-course imaging (Supplemental Figure S10) reveals that the translocation and accumulation of LDH–FITC nanoparticles in the vasculature occurred within 30–90 min after leaf infiltration. The green fluorescence of LDH–FITC nanoparticles was observed in vasculature structures and nearby mesophyll cells (Figure 3D). These nanoparticles were also observed in the vasculature system of both the inside (ROI1) and outside (ROI2) regions with respect to the site of infiltration (Figure 3D), suggesting that the infiltrated LDH nanoparticles translocate along and most probably within the veins of intact leaves.

To confirm our hypothesis that LDH–FITC nanoparticles translocate along or within the leaf vasculatures, leaves were excised from plants, and subsequently the cut point of the petiole of each excised leaf was directly immersed into a 1.5-mL microfuge tube that contained MES buffer (pH 6.0) supplemented with LDH–FITC nanoparticles. This approach was undertaken to allow the LDH nanoparticles within the MES buffer to directly enter the veins of detached leaves (Figure 4, A and B). In contrast to detached leaves treated with FITC only solution, where negligible fluorescence was observed (Supplemental Figures S11 and S12), much more intense fluorescence signals were observed in the main and secondary veins of detached leaves after 5–20 min of incubation with LDH–FITC solution (Figure 4A), and the fluorescence increased to almost four times higher in intensity at 10 h (Supplemental Figure S13). The observed fluorescence continued to migrate distally from the excised petiole tips through the vascular system of detached leaves as the period of incubation in LDH–FITC MES buffer solution was extended. For example, after 10 h of incubation, strong green fluorescence was readily observed in the main, secondary, and tertiary veins of excised leaves (Figure 4A; Supplemental Figure S12).

Cross section images of leaf midrib at 4 h after petiole application of LDH–FITC were taken to examine through

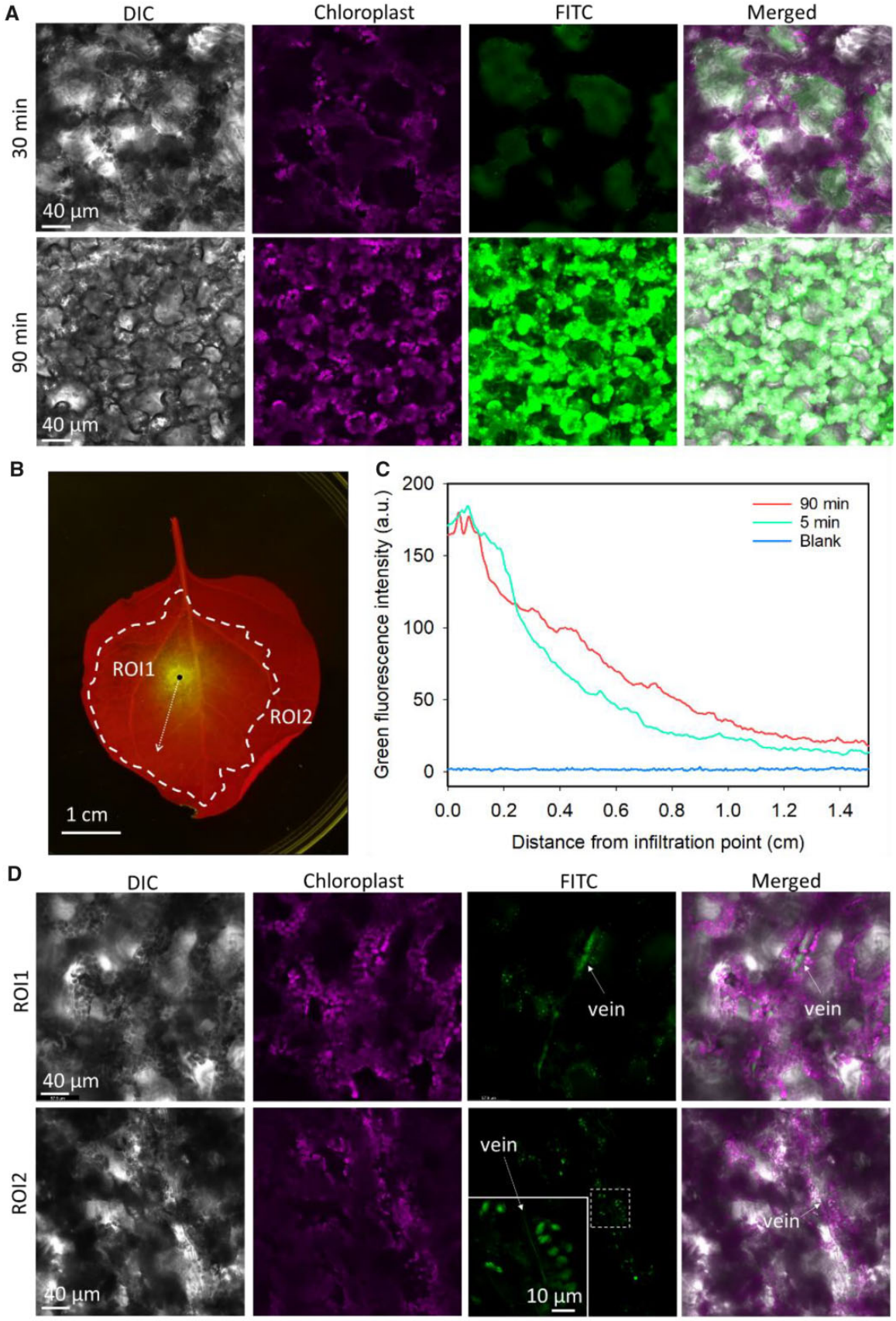

Figure 3 Internalization and translocation of LDH nanoparticles after infiltration into the whole leaf. A, Representative confocal microscope images of leaves infiltrated with LDH–FITC (100 μL, 200 mg L^{-1} LDH, 10 mg L^{-1} FITC) at 30- and 90-min post infiltration. B, Representative image of leaf infiltrated with LDH–FITC at 5 min after infiltration (red fluorescence from chlorophyll and green fluorescence from LDH–FITC). Black dot

(continued)

where the nanoparticles translocate and how they are distributed and accumulated (Supplemental Figure S14). Cell impermeable Dextran–FITC was applied as the xylem mobile only model molecule for comparison. The fluorescence of LDH–FITC nanoparticles was detected along the xylem cell wall, and in phloem and collenchyma cells below and above the xylem, respectively, as well as in leaf mesophyll cells. Some of the LDH–FITC signals in the images is likely derived from collapsed cells that were damaged during sectioning. Nevertheless, the images suggest that the LDH–FITC nanoparticles are translocated through the xylem, and possibly the phloem, into the cells around the xylem of the leaf petiole applied with LDH–FITC. On the contrary, weak Dextran–FITC signal was only observed along the xylem wall. The low fluorescence intensity inside the xylem was possibly caused by the low retention and accumulation rate of nanoparticles and molecules, due to the lack of cell organelles and complex structures in the xylem.

Further analysis showed time-dependent accumulation of LDH–FITC fluorescence intensity in the main vein of excised leaves at a distance 0.2 cm from the tube filled with LDH–FITC solution (point A, Figure 4B). An increasing accumulation of LDH–FITC signal was observed at this distance over the first 5 h of incubation, which was then followed by a plateauing at this point onward (Figure 4C). A similar curve was obtained for the main leaf vein at a distance of 1.0 cm from the tube (point B, Figure 4B); however, the increment of increased FITC fluorescence over time was relatively less

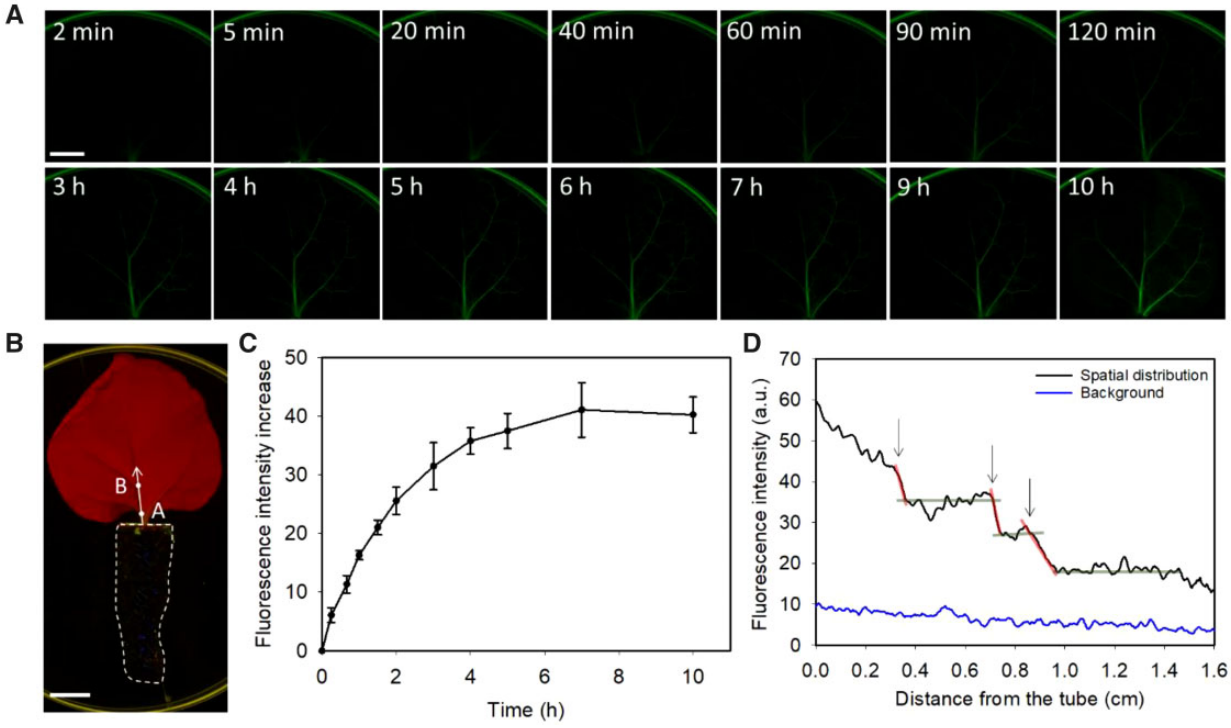

Figure 4 Translocation of LDH nanoparticles in veins of excised leaves. A, Representative images of translocation of LDH–FITC along or inside the veins of excised leaves treated with LDH–FITC (200 mg L^{-1} LDH, 10 mg L^{-1} FITC) in pH 6.0 MES buffer (bar, 1 cm). B, Representative image of the experiment system used; the petiole of the excised leaf was immersed in a tube filled with pH 6.0 MES buffer containing 200 mg L^{-1} LDH–FITC (bar, 1 cm; dashed line represents tube filled with LDH–FITC; white dots are representative points where time-dependent analysis of fluorescence was conducted; arrowed line indicates the main vein region of interest for spatial-dependent analysis of fluorescence in (D). C, Statistical data of time-dependent LDH–FITC fluorescence increase on the main vein at 0.2 cm from the tube (point A in (B)). Data represented as mean ± SEM (n = 3 biological replicates). D, Statistical analysis of spatial distribution of LDH–FITC fluorescence along the main vein of leaves (indicated by arrow in (B)) at 1 h after immersion of the excised leaves in MES buffer containing 200 mg L^{-1} LDH–FITC (n = 3 biological replicates). Steep red lines and arrows indicate sudden decrease (cliff) and flat gray lines indicate slow decrease or increase (plateau). (C and D) represent the average fluorescence intensity from three biological replicates (independent treatment on three leaves).

Figure 3 (Continued)
illustrates infiltration point; dotted arrow represents the line for analysis of nanoparticle translocation from the infiltration point (see (C)); dashed bold line indicates the boundary of infiltration area where infiltrated solution reached immediately after infiltration; ROI indicates regions of interest relative to infiltration point and infiltrated area (see (D)). C, Green fluorescence intensity at various distances from infiltration point of non-treated leaves and leaves infiltrated with LDH–FITC at 5- and 90-min post infiltration, with the average intensity based on three biological replicates (independent treatment on different leaves). D, Representative confocal microscope images of LDH–FITC (200 mg L^{-1}, 100 μL) in veins and surrounding cells inside (ROI1) and outside (ROI2) the infiltrated area of leaves at 90-min post infiltration.

with a greater statistical variation (Supplemental Figure S15). The spatial distribution of the green fluorescence (i.e. LDH–FITC nanoparticles) along the main vein at 1 h after leaf incubation in LDH–FITC solution is shown in Figure 4D. Generally, the fluorescence distribution decreased as the distance from the tube increased, although some plateaus (e.g. at 0.5–0.7 cm, 0.8–0.9 cm, and 1.0–1.4 cm as indicated by the gray lines in Figure 4D) and cliffs (e.g. at 0.3, 0.7, and 0.9 cm as indicated by red lines in Figure 4D) in the fluorescence profile deviated from the generally observed trend.

These observations collectively suggest that LDH nanoparticles translocate along the main vein and smaller secondary veins in a spatial- and time-dependent manner. The time-dependent fluorescence distribution profile generally fits Fick's Law of diffusion at each measured point in the whole vein range (0.1-cm interval from 0.1 to 1.5 cm; Supplemental Figure S15A). The average diffusion coefficient for all points were calculated to fit the spatial-dependent translocation of LDH nanoparticles along the vein with that predicted by Fick's Law of diffusion (Supplemental Figure S15 and Supplemental Table S2). The observed distance-dependent fluorescence profile generally fitted well with that predicted by Fick's Law using the average diffusion coefficient at 95% confidence level (Supplemental Figure S15, B–E), suggesting that diffusion is the main process driving the translocation of LDH–FITC nanoparticles along or within the vein. The observed deviations most likely resulted from alterations in vein structures, such as a change in vein size or the frequency of branch points along the main vein, leading to varied diffusion coefficients around these points. Alternatively, the plateaus and cliffs observed in the distance-dependent fluorescence profile along the main vein could reflect the size distribution of the LDH nanoparticles and size-dependent differences in diffusion rates of the nanoparticles.

Apart from the spreading of nanoparticles through the veins after petiole application, the nanoparticles may also translocate to other leaves and organs through the vascular system. As illustrated in Supplemental Figure S16, LDH–FITC signals were observed in the vascular system and the surrounding cells of preliminary leaves and cotyledons at 10 h after direct application of LDH–FITC nanoparticles to the excised stem of Arabidopsis seedlings.

LDH nanoparticles deliver nucleic acid to leaf cells

Cy5-labeled 21-bp DNA (Cy5–DNA, listed in Supplemental Data Set S1) was initially used as a model nucleic acid for conjugation with LDH nanoparticles (LDH–Cy5–DNA, 100 mg·L^{-1} of LDHs and 10 mg·L^{-1} of Cy5–DNA). LDH–Cy5–DNA suspension was infiltrated into the abaxial side of leaves of the *N. benthamiana* transgenic line 16c, which constitutively expresses a *GFP* transgene. At 90-min post LDH–Cy5–DNA infiltration, the leaves were imaged using a confocal microscope (Figure 5A), and the captured images were used to determine the relative amount of Cy5–DNA uptake by plant cells. The Cy5–DNA internalization ratio

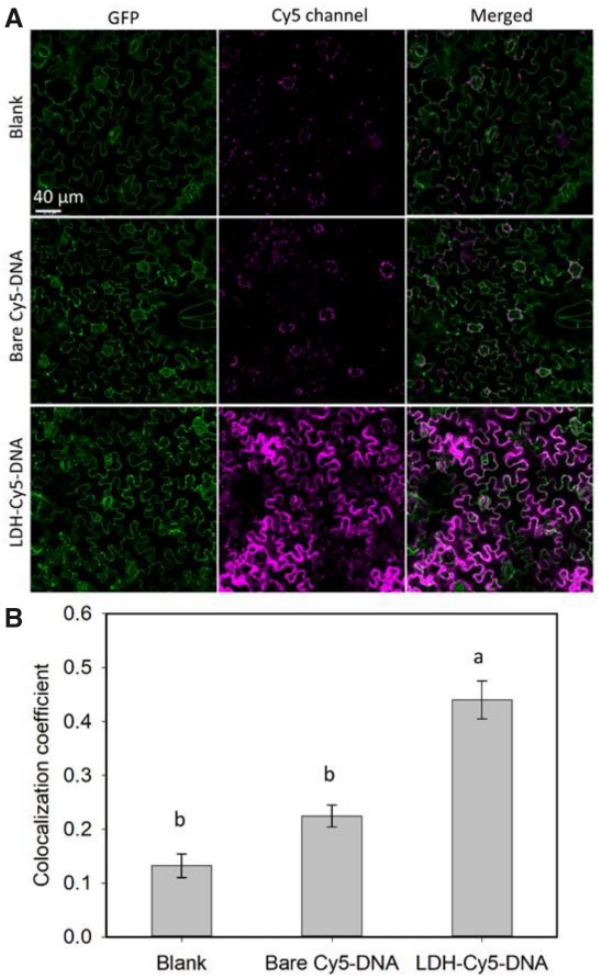

Figure 5 Cy5–DNA delivery by LDHs into leaf epidermis cells of GFP-expressing transgenic *N. benthamiana* line 16c. A, Representative confocal images of untreated leaves and leaves infiltrated with Cy5-DNA (10 mg L^{-1}) and LDH–Cy5–DNA (100 mg L^{-1} LDH, 10 mg L^{-1} Cy5–DNA) at 90-min post infiltration. B, Statistical colocalization coefficient, for example Pearson's correlation coefficient of Cy5 with intracellular GFP, $n = 3$ (independent infiltration on three leaves from three plants). The lower-case letter with the bar indicates statistical significance with $P < 0.05$, by one-way ANOVA with post hoc Tukey's analysis, data represented as mean ± SEM.

was quantified through measuring the colocalization coefficient between magenta Cy5 fluorescence and the institutive GFP, which was adopted as the indicator of the intracellular cytosol (Figure 5B).

There was only a weak magenta background fluorescence in leaves infiltrated with blank MES. The weak Cy5-like signals in the blank control is mainly attributed to interference stemming from the background chlorophyll fluorescence. In contrast, a very strong magenta fluorescence signal was observed for leaves infiltrated with LDH–Cy5–DNA at 90-min post infiltration (Figure 5A). Relatively, infiltration of the equivalent amount of naked Cy5–DNA resulted in only weak magenta fluorescence in some leaf cells, which was

mostly concentrated around the periphery of stomata (Figure 5A; Supplemental Figure S17). These observations further indicate that infiltrated LDH–Cy5–DNA nanoparticles were rapidly taken up by the leaf cells. The time-dependent internalization images (Supplemental Figure S18) also reveal that LDH–Cy5–DNA effectively entered and accumulated in the abaxial epidermal cells within 3 h of infiltration, while the naked Cy5–DNA could not be efficiency taken up by the abaxial cells of *N. benthamiana* leaves.

The control leaves had an average colocalization coefficient of 0.13 ± 0.02 between the Cy5 and GFP channels (Figure 5B), with the residual Cy5-like signal being attributed to the autofluorescence of chlorophyll. Leaves infiltrated with LDH–Cy5–DNA showed the highest colocalization coefficient of 0.44 ± 0.04, which was significantly higher than that determined for leaves infiltrated with naked Cy5–DNA alone (0.22 ± 0.02) and blank control leaves (0.13 ± 0.02). These data indicate that LDH nanoparticles efficiently delivered their Cy5–DNA cargo into the leaf cells. In contrast to the value obtained for leaves infiltrated with LDH–Cy5–DNA, the Cy5–GFP colocalization coefficient of leaves infiltrated with naked Cy5–DNA was not statistically different from that of the blank control leaves (Figure 5B), a finding that again suggests that naked nucleic acid is either difficult for intact plant cells to internalize, or is rapidly degraded prior to its entry into the leaf cells (Demirer et al., 2020; Zhang et al., 2021). Therefore, the enhanced uptake of LDH-conjugated nucleic acids into leaf cells can be attributed to the rapid internalization of the LDH carrier, together with protection of the nucleic acid cargo from extracellular endonucleases by the LDH nanoparticles (Supplemental Figure S19A).

RNA interference induced by LDH delivered siRNA

We next infiltrated *GFP*-specific siRNA duplexes (sequences provided in Supplemental Data Set S2), either naked or in complex with LDH nanoparticles, into the leaves of the *N. benthamiana* 16c plant line to compare their capacity to induce *GFP* silencing. As the 16c line constitutively expresses *GFP*, the silencing of *GFP* can be qualitatively and quantitatively assessed via the measurement of GFP fluorescence by confocal microscopy and the mRNA level, as well as the subsequent statistical analysis of the captured images.

Initially, 50 μL of LDH–siRNA suspension at a siRNA concentration of 800 nM (~5-μg siRNA was delivered per leaf) was gently infiltrated onto the abaxial side of fully expanded 16c leaves. An obvious reduction in GFP fluorescence was observed 3 days after infiltration with LDH–siRNA nanoparticles (Figure 6A), suggesting that siRNA delivered by LDH nanoparticles successfully silenced the expression of the GFP transgene. In contrast, infiltration of 16c leaves with naked siRNA and/or with LDH nanoparticles conjugated with non-specific siRNA (LDH–ns-siRNA) resulted in almost no change in the level of GFP fluorescence compared to noninfiltrated (blank) 16c leaves. As shown in Figure 6B, increasing

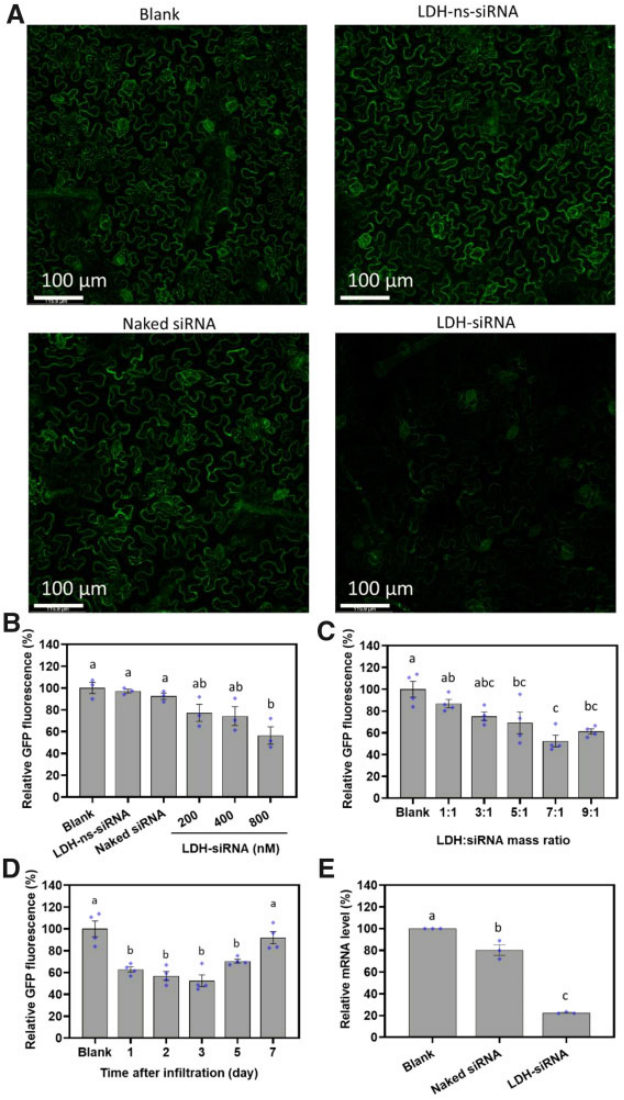

Figure 6 GFP gene silencing induced by LDH-delivered siRNA in GFP-expressing transgenic *N. benthamiana* line 16c. A, Representative confocal microscope images of nontreated (Blank), LDH conjugated nonspecific siRNA (LDH–ns-siRNA), naked siRNA (800 nM), and LDH complexed siRNA (LDH–siRNA, LDH: siRNA mass ratio at 7:1, siRNA concentration of 800 nM) infiltrated (50 μL) 16c leaves 3-day post infiltration. B, Quantitative GFP fluorescence intensity from confocal images for nontreated leaves and leaves infiltrated with 50-μL LDH–ns-siRNA (800-nM siRNA), naked siRNA (800 nM), and LDH–siRNA at the siRNA concentration of 200, 400, and 800 nM and LDH:siRNA mass ratio of 7:1, 3-day post infiltration. C, Quantitative GFP fluorescence intensity of leaves infiltrated with LDH–siRNA (50 μL, 800-nM siRNA concentration) at different LDH: siRNA mass ratios. D, Time-dependent GFP fluorescence intensity of leaves infiltrated with LDH–siRNA (50 μL, 800-nM siRNA, LDH: siRNA mass ratio at 7:1). E, RT–qPCR analysis for *GFP* mRNA levels at Day 1 post infiltration for leaves infiltrated with naked siRNA or LDH–siRNA, data were normalized based on housekeeping gene *elongation factor 1* and the nontreated leaf (Blank). B–E, Different lower-case letters above the bars represent statistical significance with $P < 0.05$ in one-way ANOVA with post-hoc Tukey's analysis. Data represented as mean ± SEM. The diamonds indicate individual biological replicates.

LDH–siRNA concentration from 200 to 800 nM (LDH:siRNA mass ratio of 7:1) progressively increased the degree of silencing of GFP expression. More specifically, at 3-day post infiltration, 800 nM of siRNA loaded on LDH nanoparticles significantly decreased the GFP fluorescence to 56.5% ± 7.9% of the untreated 16c control leaves (Figure 6B), while 200 and 400 nM of siRNA loaded onto LDH nanoparticles decreased the GFP fluorescence (77.2% ± 7.8% and 74.2% ± 8.6%, respectively), but not significantly. In contrast, at 3-day post infiltration, the level of GFP fluorescence of leaves treated with either 800-nM naked siRNA (92.5% ± 2.8%) or with 800-nM LDH–ns-siRNA control (91.2% ± 1.7%) was not significantly different from the noninfiltrated 16c control leaves (Figure 6B, with corresponding one-way analysis of variance (ANOVA) details in Supplemental Table S3).

Figure 6C (corresponding one-way ANOVA details in Supplemental Table S4) shows that the concentration of the LDH nanoparticles in the LDH–siRNA complex (with the same amount of siRNA) also significantly influenced the degree of inhibition of GFP expression. Specifically, increasing the loading mass ratio of LDH:siRNA from 1:1 to 7:1 incrementally reduced GFP expression from 86.7% ± 3.8% to 52.5% ± 5.3%, indicating that LDH nanoparticles were essential for the induction of efficient silencing of GFP expression in planta. The greatest reduction to GFP fluorescence was observed at an LDH:siRNA mass ratio of 7:1. The siRNA was completely loaded onto the LDH nanoparticles at a loading mass ratio of 7:1, and as the LDH:siRNA mass ratio was experimentally decreased in increments down to 1:1, there was an increasing amount of free siRNA detected in solution (Supplemental Figure S19B), as well as a reduction to the degree to which GFP expression was silenced (Figure 6C). On the other hand, the group with the ratio of 9:1 showed a slightly lower silencing efficiency (61.2% ± 2.4%) compared to that of 7:1 (52.5% ± 5.3%), which may be attributed to two reasons. First, more LDHs were used to load the same amount of siRNA at 9:1, which may have slowed the uptake efficacy of siRNA compared to that at 7:1 as each nanoparticle loaded much less siRNA molecules (Wu et al., 2018). Second, after entering the plant cells, the release of siRNA from LDH–siRNA at 9:1 is predicted to be much slower than that at 7:1 (Supplemental Figure S19C) in the similar slightly acidic environment, thus relatively less siRNA is available for the silencing of target mRNA in the plant cytoplasm (Figure 6C).

A time-dependent analysis of GFP fluorescence was conducted to reveal the kinetics of GFP silencing (Figure 6D). A significant decrease in GFP fluorescence was observed 1-day post infiltration of 16c leaves with 800-nM siRNA in complex with LDH nanoparticles (down to 62.8% ± 2.4% of the blank control), followed by 56.9% ± 4.0% at day 2 and 52.5% ± 5.3% at day 3, indicating a rapid internalization by the plant cells and subsequently quick silencing of the expression of the targeted *GFP* transgene by LDH-delivered siRNA (corresponding one-way ANOVA details in Supplemental Table S5). The decrease in GFP fluorescence was maintained until 5-day post infiltration with GFP expression still reduced to a level of 70.3% ± 1.8% of the blank control. However, GFP fluorescence was observed to recover to a level which was almost the same intensity as the nontreated 16c control group had at day 7 post infiltration (91.9% ± 5.5%). Together, these data reveal that the silencing of GFP by LDH-delivered siRNA is a transient process that lasts for approximately 5–7 days post nanoparticle application, at which timepoint the efficacy of silencing starts to decline. This transient silencing for 5–7 days has been also reported with carbon nanotube delivered siRNA (Demirer et al., 2020).

The silencing of *GFP* at the mRNA level was additionally demonstrated by use of a standard reverse transcription–quantitative polymerase chain reaction (RT–qPCR) approach, with the abundance of the *GFP* transcript decreasing even further than the amount of GFP protein. As illustrated in Figure 6E, there was only a slightly significant decrease (19.8% ± 4.9%) in the abundance of the *GFP* transcript at day 1 post infiltration for 16c leaves treated with 800-nM naked siRNA (corresponding one-way ANOVA details in Supplemental Table S6). In direct contrast, leaves infiltrated with the same concentration of siRNA in complex with LDH nanoparticles showed a much more significant decrease to the abundance of the *GFP* transcript. Namely, the abundance of the *GFP* transcript was reduced by 77.4% ± 0.5% in LDH:siRNA infiltrated leaves compared to the level of this transcript in the leaves of 16c control plants. Collectively, these results demonstrate LDH nanoparticles readily facilitate the internalization of loaded siRNAs, which in turn enhance the efficacy of GFP silencing in 16c leaves.

Discussion

Nanoparticle-mediated delivery of biomolecules is gaining momentum for plant science and agricultural applications (Raliya et al., 2018; Zhao et al., 2020), with various advantages including feasibility, biocompatibility, and controlled release of the cargo (Landry and Mitter, 2019). While most investigations on nanoparticle entry into plant cells have focused on the environmental and biological impact of nanoparticles (Lv et al., 2019; Su et al., 2019), there have been few reports about applying nanoparticles as carriers for the delivery of biomolecules into plants cells. Carbon nanotubes and mesoporous silica nanoparticles have been investigated in this emerging field to date. In comparison to these nanoparticles, LDH nanosheets can be prepared and modified at low cost, and have now demonstrated superior biocompatibility and efficiency when used as nanocarriers for biomedical applications. Moreover, our previous report has also demonstrated that when LDH nanoparticles in complex with long viral-dsRNA were delivered onto leaves, the period of protection against homologous viruses was lengthened by up to a month due to the slow release of dsRNA on the leaf surface via slow degradation of the LDH nanoparticles (Mitter et al., 2017). However, these LDH nanoparticles were shown to rarely enter the leaf cells post their surface

spraying, probably due to the barrier of the hydrophobic cuticle layer on the leaf surface. Our recent study has demonstrated that LDH–dsRNA nanoparticles of up to 50 nm in diameter can be taken up to induce RNAi in isolated pollen (Yong et al., 2021). However, the uptake and translocation of LDH nanoparticles in whole plant leaves have not been investigated yet. In this study, we have shown that smaller LDH nanoparticles with the average size range of ~40 nm can be introduced into whole leaves through infiltration and, importantly, post their application, the smaller LDH nanoparticles are readily internalized by the intact cells and chloroplasts of the infiltrated leaves. We have also demonstrated that LDH nanoparticles diffuse through the apoplast, and in particular, within the veins of the leaf, possibly through both the xylem and the phloem, a finding which provides considerable mechanistic insights into plant–nanoparticle interactions. We have further revealed that these smaller LDH nanoparticles efficiently deliver siRNA cargo into the cells of the infiltrated leaf, and that the delivered siRNAs are functionally active in directing silencing of the expression of the targeted *GFP* transgene in planta.

As illustrated in Figure 7 and based on the experimental data presented here, we propose that the LDH–siRNA nanoparticles experience the following processes after infiltration into the leaf. Specifically, LDH–siRNA upon infiltration: (1) enter the apoplast; (2) diffuse and translocate within the apoplast and the vasculature; (3) are internalized by mesophyll and epidermal cells; (4) enter chloroplasts and other subcellular organelles; and (5) in the cytoplasm, release their siRNA cargo via degradation of LDH nanoparticles, which can act as functional molecules to direct efficient silencing of targeted genes. Furthermore, the infiltrated LDH nanoparticles are first driven through the apoplast in the infiltration area by the infiltration pressure, initially through the spongy mesophyll tissue, and then continue to diffuse further through the apoplast. Their diffusion rate through the apoplast is size dependent, allowing smaller nanoparticles to move freely away from the infiltration point but retaining larger nanoparticles around the point of infiltration. The diffusion of smaller quantum dot nanoparticles (3–5 nm) is much quicker and much more uniform throughout the infiltrated tissue (Supplemental Figure S9), a finding that strongly suggests that the size-dependent diffusion is not controlled by a single size exclusion limit within the apoplast translocation pathway (Lv et al., 2019; Dietz and Herth, 2011). Rather than restricting nanoparticle movement according to a single size exclusion limit, our data indicate that the apoplast acts as a matrix and the diffusion rate of nanoparticles is inversely proportional to their size. We have also observed LDH nanoparticles in the vasculature structures far from the infiltration point and even in noninfiltrated areas of the leaf (Figure 3D), suggesting that LDH nanoparticles may utilize the veins to translocate to other parts of the leaf and perhaps throughout the plant, similarly to the reports that some nanoparticles translocate to the shoot after uptake by the root or trunk injection (Sun et al., 2014; Su et al., 2020). The translocation along the vein has been confirmed by incubating excised leaves and shoots in an LDH-containing suspension. As observed in this research, nanoparticles may translocate through both the xylem and the phloem (Supplemental Figure S14), which could be valuable to aid RNA cargos to overcome the limits of translocation in the petiole and the leaf vein through the xylem and apoplast (Dalakouras et al., 2018). Overall, the movement of LDH nanoparticles into the detached leaves and along the veins follows Fick's Law of diffusion (Supplemental Figure S15). These findings suggest that diffusion is a major driving force for the movement of LDH nanoparticles along the veins of leaves.

During the diffusion and translocation through the leaf, LDH nanoparticles are efficiently taken up by mesophyll and epidermal cells. The internalization of nanoparticles by intact leaf cells was already evident at 90 min after infiltration, with a substantial number of LDH–FITC nanoparticles taken up by leaf cells (Figure 3A). The high diameter to thickness ratio (6–7), the high positive charge, and the stiffness of LDH nanoparticles, together with the highly electronegative nature of the inner surface of the plant plasma membrane, may contribute to the effective and rapid internalization

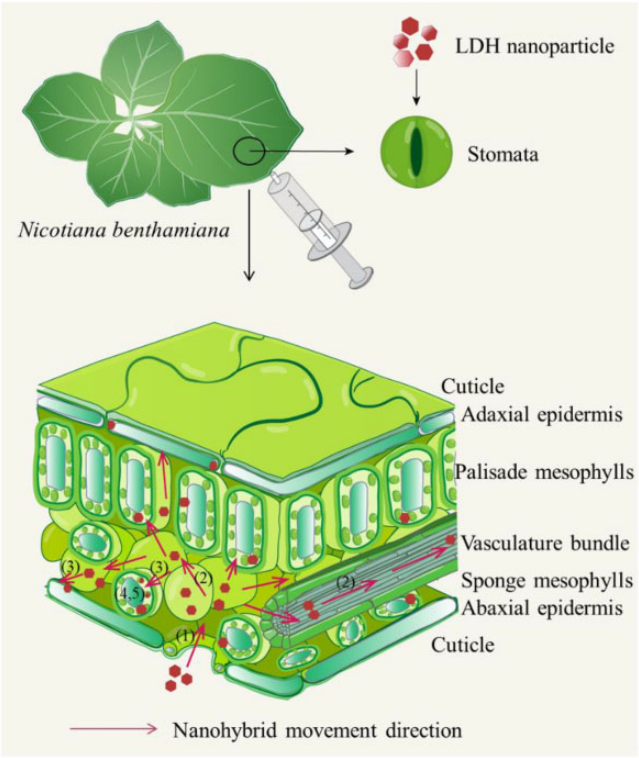

Figure 7 Schematic illustration of internalization and translocation of LDH nanoparticles in leaves after infiltration. (1) LDH nanoparticles enter the apoplast region after infiltration; (2) LDH nanoparticles diffuse and translocate within the apoplast region and along the vein; (3) LDH nanoparticles are internalized by mesophyll and epidermis cells; (4) LDH nanoparticles bind to chloroplasts and other negatively charged organelles; and (5) LDH nanoparticles release siRNA, inducing silencing of the target gene.

of these nanoparticles by plants cells (Xu et al., 2007; Zhang et al., 2019; Yong et al., 2021). In contrast, the weak green fluorescence of leaves infiltrated with free FITC (Figure 2) may be caused by limited cellular uptake, and moreover, the quenching of free FITC fluorescence in the acidic apoplastic region of the leaf (Lanz et al., 1997; Martiniere et al., 2018). Note that free FITC anions are only strongly fluorescent in neutral to basic buffers (pH 7–9), but emit very weak fluorescence in pH 5.0–6.5 buffers due to the cyclization of fluorescein into a lactone form (pKa, 6.7; Zhao et al., 1989). Since FITC anions are intercalated within LDH interlayers, they continue to fluoresce strongly even in pH 5–7 buffers as they are protected within the layers (Supplemental Figure S20). Thus, free FITC contributed very little green fluorescence compared with LDH–FITC nanoparticles when infiltrated into the acidic apoplast environment of the leaf (pH ~6; Martiniere et al., 2018). On the other hand, free FITC would be expected to fluoresce strongly at pH ~7.5 in the plant cytoplasm, and therefore, the lack of strong florescence after applying free FITC in the leaf suggests that free FITC is not readily internalized by cells of infiltrated *N. benthamiana* leaves, unlike LDH–FITC nanoparticles.

An interesting phenomenon revealed in this research is that LDH–FITC nanoparticles are not only internalized by intact plant cells, but also subsequently colocalize with chloroplasts in the cytoplasm of leaf cells. This observation suggests that LDH nanoparticles can penetrate into the subcellular organelles after entering the mesophyll cells. This finding is in accordance with the previous report that positively charged nanoparticles penetrate through the cell membrane and colocalize with chlorophyll in the chloroplast (Giraldo et al., 2014; Lew et al., 2018). The positively charged nature of LDH nanoparticles (Supplemental Table S1) may increase their affinity for the negatively charged membrane of chloroplasts, enabling LDH nanoparticles to act as potential carriers of biomolecules, which themselves carry a negative charge (e.g. DNA and RNA), into these negatively charged subcellular membrane structures.

We have further demonstrated that LDH nanoparticles efficiently delivered 21-bp DNA and siRNA duplexes into *N. benthamiana* leaf cells. We have shown that LDH delivered Cy5–DNA into the cytosol of the leaf epidermis, as fluorescence of Cy5 colocalized with intracellular GFP signal of 16c leaf cells. More specifically, LDH nanoparticles delivered siRNA to silence the expression of the *GFP* transgene in the leaves of the 16c plant. Indeed, LDH–siRNA (7:1) reduced the GFP florescence by 37.2% ± 2.4%, and the abundance of the *GFP* transcript by 77.4% ± 0.5%, a single day post the application of the LDH–siRNA complex (Figure 6, D and E), with the observed silencing of GFP expression in 16c leaves continuing to be observed for 5- to 7-day post infiltration. Enhanced silencing induced by LDH–siRNA nanoparticles can be attributed to rapidly facilitated internalization of the nucleic acid and the protection offered to the delivered siRNA cargo from endonuclease degradation (Demirer et al., 2020). Furthermore, the slow release of *GFP*-specific siRNA from LDH nanoparticles within the cytosol (Chen et al., 2018a) sustained the efficient knockdown of GFP expression for ~5–7 days after the leaf was infiltrated. This demonstrates that the slow release and the biodegradability characteristics of LDH nanoparticles should make it possible to lengthen the period between repeat applications of LDH nanoparticles in order to maintain sustained silencing of a targeted gene.

In summary, the current research shows that rapid internalization of 40-nm LDH nanoparticles and the concomitant protection of nucleic acid cargo against degradation by endonucleases enable the successful delivery of siRNA to silence the expression of a targeted gene in an intact plant cell. Thus, LDH nanoparticles are feasible carriers of biomolecules, not only for plant protection from viruses (Mitter et al., 2017) and other plant pathogens (Bugatti et al., 2019), but also for the study of metabolic pathways and the modification of desirable agronomic traits in plants. The chloroplast penetrating ability of LDH nanoparticle makes it a potential carrier for biomolecule delivery to subcellular structures and compartments. Moreover, our results suggest that the LDH-based delivery platform can potentially be used to deliver other forms of RNA, including mRNAs for the expression of specific proteins and guide RNAs for specific gene editing purposes in intact plant cells.

Materials and methods

LDH nanoparticles synthesis and characterization

The synthesis of MgAl LDH nanoparticles was slightly modified from the previously reported co-precipitation method (Xu et al., 2006a). Briefly, $Mg(NO_3)_2$ and $Al(NO_3)_3$ methanol solution were added into NaOH methanol solution under constant stirring for 20 min, the mixture was then washed once with methanol and once with deionized water, and the collected slurry was dispersed in deionized water. The as-prepared suspension was then heated in autoclave at 100°C for 30 min to obtain well dispersed LDHs. FITC-labeled LDHs (LDH–FITC) were prepared by stirring LDH nanoparticles with FITC solution (LDH:FITC mass ratio was 20:1) for 1 h, allowing FITC to intercalate into LDH interlayers (Supplemental Figure S20). The FITC-loaded nanoparticles were washed three times to remove free FITC and then redispersed in deionized water.

The size distribution and the surface charge were measured in a Zetasizer Nano (Malvern Panalytical) with the DLS method. The TEM images were obtained in a JEOL JSM-2010. Over 200 individual particles were documented for the size distribution and number-mean size estimation. XRD pattern of lyophilized LDH sample was collected with a Rigaku Miniflex X-ray diffractometer at a scanning rate of 2°/min using Cu $K\alpha_1$ radiation.

Plant growth conditions

Nicotiana benthamiana (nontransgenic wild-type and *GFP* transgenic line 16c) were germinated and grown in the

growth room at the day temperature of 20°C–22°C and the night temperature of 16°C–18°C (12 h/12 h) with artificial light. The plants were grown in UQ23/UC mix (50/50 v/v) mixture soil. *Arabidopsis thaliana* (Col-0) plants were vertically grown in Murashige–Skoog solid medium in culture dish in growth room.

Leaf infiltration and uptake of LDH nanoparticles by excised shoot, leaves, and chloroplasts

LDH nanoparticle suspension (50–100 μL) or other solution in 20-mM pH 6.0 MES buffer was infiltrated from the abaxial surface of leaves (5–7 weeks) with 1-mL needleless syringe slowly. Then kimwipe was used to gently remove residue liquid on the leaf surface. Note that the infiltrated leaves were attached to the plant and kept in the growth room until collection for analysis. In LDH–FITC and LDH–Cy5–DNA infiltration experiments, the plants were covered with aluminum-foil-lined plastic lids to keep from lights after infiltration. For LDH's biocompatibility analysis, 100 μL of LDHs (200 μg mL^{-1}) and 100-μL 1% (v/v) SDS were infiltrated into leaves and subjected to confocal microscope imaging to check the leaf cell integrity after 1 h.

Chloroplasts extraction was performed by grinding *N. benthamiana* leaves in chilled extraction buffer (0.33-M sorbitol, 0.1-M Tris–HCl, pH 7.8, 5-mM $MgCl_2$, 10-mM NaCl, 2-mM EDTA) followed by filter through a 70-mesh cell strainer. The suspension was centrifuged at 200 *g* for 3 min, the supernatant was collected and centrifuged at 1,000*g* for 7 min. The obtained chloroplast pellet was dispersed in pH 6.0 MES buffer supplemented with FITC or LDH–FITC.

For experiments on excised leaved, the petiole was cut 0.5 cm from the leaf blade and the cut point of the petiole of each excised leaf was immersed into a 1.5-mL microfuge tube that contained MES buffer (pH 6.0) supplemented with 200 mg·L^{-1} of LDH–FITC or the equivalent concentration of free FITC. The tube was capped with parafilm to prevent evaporation and covered with aluminum foil to prevent photobleaching of FITC.

For excised Arabidopsis shoot uptake assay, 2-week-old Arabidopsis seedlings were removed from growth medium, cut at 2–3 mm below the meristem and hanged in a 96-well plate filled with 20 mM of MES buffer (pH 6.0) supplemented with 200 mg·L^{-1} of LDH nanoparticles, with only lower part of the stem immersed into culture media.

Nucleic acid loading/release assay and RNase protection assay

LDH nanoparticles were dropwise added into nucleic acid suspensions (DNA and siRNA, sequences provided in Supplemental Data Sets S1 and S2) at the designed LDH/nucleic acid mass ratio, followed by pipette mixing and aging at room temperature for 2 h to allow maximal conjugation of nucleic acids onto LDH particles. Electrophoresis was applied to test if nucleic acids were conjugated to LDHs. Gel electrophoresis was run at 80 V for 30 min on 2% (w/v) agarose gel.

In RNase protection assay, 250-ng siRNA was firstly loaded with 1,750 ng of LDHs (LDH–siRNA, LDH:siRNA mass ratio of 7:1). RNase A (5 ng, Thermo Fisher) was added into the suspension and incubated at 37°C for 5 min. siRNA was then released with release buffer (4.11 mL of 0.2-M Na_2HPO_4 and 15.89 mL of 0.1-M citric acid; pH 3) after treatment and then subjected to electrophoresis to test the siRNA degradation fraction.

In acidic environment release assay, 250-ng siRNA was firstly loaded with 1,750 and 2,250 ng LDHs (7:1 and 9:1) and aged at room temperature for 2 h. Then the mixed suspension (LDH–siRNA) was transferred to pH 6.0 MES buffer and incubated at room temperature for one day and subjected to electrophoresis to test the release.

LDH delivery of siRNA to induce RNAi and GFP fluorescence quantification

LDH–siRNA and LDH–ns-siRNA control (sequence provided in Supplemental Data Set S2) were prepared by mixing LDHs with siRNA solution as described above. Naked siRNA (50 μL) and LDH–siRNA (50 μL) were suspended in MES buffer and infiltrated into well expanded 16c leaves (5–7 weeks). The infiltrated plants were placed in the growth room for 1, 2, 3, 5, 7 days and then harvested for tests. The quantitative analysis of GFP expression level was conducted based on confocal microscope images, three to four biological replicates of individual leaves from different plants were performed for each group, and five nonoverlap fields of view focuses on the epidermal layer were measured and averaged to obtain the value of each replicate. The analysis data were normalized based on the average intensity of untreated group (Blank).

Total mRNA extraction and RT–qPCR analysis

The whole infiltrated leaves were detached from the plants and ground into fine powder in liquid nitrogen and subjected to RNA extraction. Total RNA extraction from leaves was performed with TRIzol Reagent (ThermoFisher) following the manual instruction. Reverse transcription of extracted total mRNA was conducted with ProtoScript II First Strand cDNA Synthesis Kit (New England Biolabs). *GFP* was selected as the target gene and *EF1* (*elongation factor 1*) as the reference housekeeping gene, the primer sequences were listed in Supplemental Data set S3. The RT–qPCR was set to run 40 cycles with annealing temperature 60°C. The *GFP* mRNA level was normalized based on *EF1* housekeeping gene mRNA level and blank control with ΔΔCt method.

Fluorescence parameters

For confocal imaging of leaves, FITC signal was detected with λ_{ex} = 490 nm, λ_{em} = 500–600 nm, laser intensity 100%, gain at 800, and the lower limit of 15 to exclude auto-fluorescence; chlorophyll signal was detected with λ_{ex} = 490 nm, λ_{em} = 600–750 nm, laser intensity 100%, and gain at 800; Cy5 signal was detected with λ_{ex} = 645 nm, λ_{em} = 655–750 nm, laser intensity 3%, and gain at 100 with HyD detector applied; GFP signal was detected with

λ_{ex} = 480 nm, λ_{em} = 490–590 nm, laser intensity 5%, and gain at 100 with HyD detector applied. The images were taken on a Leica SP8 Laser Scanning Confocal Microscopy under 40× objective magnification. For GFP fluorescence intensity analysis in silencing experiment, confocal microscope images were taken under 10× objective magnification with λ_{ex} = 480 nm, λ_{em} = 490–600 nm, laser intensity 10%, and gain at 100 with HyD detector applied. High-resolution chloroplast images were taken with 100× objective magnification with λ_{ex} = 490 nm, laser intensity 100%; FITC signal was obtained at λ_{ex} = 490 nm, λ_{em} = 500–600 nm, gain at 300 with HyD detector applied, and the lower limit of 20 to eliminate the interference of auto-fluorescence of leaves; Chlorophyll signal was obtained at λ_{ex} = 490 nm, λ_{em} = 650–750 nm, and gain at 100 with HyD detector applied. The images were processed with Leica LasX, and the quantitative GFP fluorescence analysis was performed in ImageJ by direct measuring the average intensity of GFP channel of the whole picture.

The leaf photographs were taken on a Cannon EOS 600D equipped with an orange filter, excited with blue light provided by 4 Dark Reader Hand Lamps (Clare Chemical Research), and the aperture was set at F7.1 and the exposure time 20 s. The background deduction by channel splitting and fake color were uniformly done with ImageJ.

Colocalization analysis

The colocalization fraction between the GFP and Cy5 channels, and between the FITC and chloroplast channels in confocal images was quantified through ImageJ based on Pearson's correlation coefficient. The ratio is normalized where "1" stands for perfect colocalization and "0" for no colocalization. Three biological replicates of individual leaves collected from different *N. benthamiana* plants were infiltrated, and three nonoverlapping fields of view focused on epidermal and mesophyll cells were measured and averaged for each replicate.

Statistical analysis

Data are represented as mean ± standard error of mean (SEM). Statistical significance was analyzed through one-way ANOVA with Bartlett's test and Brown–Forsythe test to confirm the consistence of deviation and post hoc Tukey's multiple comparisons for significance between each group.

Supplemental data

The following materials are available in the online version of this article.

Supplemental Figure S1. Representative TEM images. Representative TEM image of A, LDH–FITC and B, LDH–siRNA.

Supplemental Figure S2. Confocal images of *N. benthamiana* leaves at 90 min after infiltration with 200 mg·L^{-1} LDH–FITC (100 μL).

Supplemental Figure S3. Statistical colocalization coefficient of FITC with chloroplasts estimated with Pearson's correlation coefficient, $n = 3$ (different lower-case letters above the bars indicate statistical significance with $P < 0.05$, by one-way ANOVA with post-hoc Tukey's analysis, data represented as mean ± SEM).

Supplemental Figure S4. Representative confocal images of isolated chloroplasts, showing internalization of LDH–FITC after co-incubation with 200 mg·L^{-1} LDH–FITC for 90 min.

Supplemental Figure S5. Representative confocal microscope images of 4-week-old wheat leaf cells internalization of LDH–FITC after infiltration of 25 μL 200 mg·L^{-1} LDH–FITC for 90 min.

Supplemental Figure S6. Biocompatibility of LDH nanoparticles.

Supplemental Figure S7. Representative confocal images of LDH–FITC entering abaxial mesophyll cells from the extracellular region at ∼30 min after infiltrated with 100 μL of LDH–FITC (200 mg·L^{-1}).

Supplemental Figure S8. Representative confocal images of adaxial side mesophyll and epidermal cells, showing internalization of LDH–FITC at 90 min after infiltrated with 100 μL of LDH–FITC (200 mg·L^{-1}).

Supplemental Figure S9. Blue light excited images of leaves infiltrated with different nanoparticles.

Supplemental Figure S10. Time-course confocal microscope images of LDH–FITC showing translocation and accumulation in vasculatures after infiltration of LDH–FITC (200 mg·L^{-1}, 100 μL) and possible translocation direction (white arrow).

Supplemental Figure S11. Representative images of detached leaves treated with 10 mg·L^{-1} FITC solution in pH 6.0 MES buffer (bar, 1 cm).

Supplemental Figure S12. Excised leaves petiole treated with nanoparticles.

Supplemental Figure S13. Time-dependent fluorescence increase on the main veins at 1.0 cm away from the tube containing LDH–FITC (point B in Figure 4B and white dot in Supplemental Figure S11A) and FITC (white dot in Supplemental Figure S12B).

Supplemental Figure S14. Cross-sectional images of FITC signals in midrib of *N. benthamiana* 1 cm from petiole, 4 h after petiole application of 200 mg·L^{-1} LDH–FITC and 10 mg·L^{-1} Dextran-FITC.

Supplemental Figure S15. Time- and spatial-dependent translocation and accumulation of LDH–FITC in veins.

Supplemental Figure S16. Representative confocal images of LDH–FITC translocated to 2-week-old *A. thaliana* seedling cotyledon and young leaf, 10 h after application of 200 mg·L^{-1} LDH–FITC on stem of excised shoot.

Supplemental Figure S17. Representative confocal images of infiltrated Cy5–DNA (100 μL, 10 mg·L^{-1}) localized around abaxial side stomata and in stomata chock at 1.5-h post-infiltration.

Supplemental Figure S18. Representative confocal images of time-dependent internalization by leaf abaxial epidermal cells after infiltrated with LDH–Cy5–DNA and Cy5–DNA (100 μL, 10 mg·L^{-1} of Cy5–DNA).

Supplemental Figure S19. Gel images on LDH loading, protection, and release of siRNA.

Supplemental Figure S20. Schematic illustration of FITC intercalated into LDH nanoparticles.

Supplemental Table S1. Summary of characteristic properties of LDH, LDH–FITC, and LDH–siRNA.

Supplemental Table S2. Simulated diffusion coefficient (D) and regression coefficient (R^2) of time-dependent curve at each point with 0.1-cm interval.

Supplemental Table S3. Detail data of GFP gene silencing induced by LDH-delivered siRNA in Figure 6B.

Supplemental Table S4. Detail data of GFP gene silencing induced by LDH-delivered siRNA in Figure 6C.

Supplemental Table S5. Detail data of GFP gene silencing induced by LDH-delivered siRNA in Figure 6D.

Supplemental Table S6. Detail data of GFP gene silencing induced by LDH-delivered siRNA in Figure 6E.

Supplemental Data S1. Cy5–DNA sequence (5′–3′).

Supplemental Data S2. siRNA sequence (5′–3′).

Supplemental Data S3. RT–qPCR primers (5′–3′).

Acknowledgments

The authors acknowledge Dr Andrew Eamens for his insightful suggestions. The authors acknowledge Wikipedia for inspiration on the scheme illustration. The authors also acknowledge the facilities, and the scientific and technical assistance of the Australian Microscopy & Microanalysis Research Facility at the Centre for Microscopy and Microanalysis, Australian National Fabrication Facility (ANFF, Qld Node), The University of Queensland and Microscopy facility at Institute for Molecular Bioscience, The University of Queensland.

Funding

The authors acknowledge the support from Australian Research Council Discovery Project (DP190103486) and Research Hub (IH190100022), and National Health and Medical Research Council (APP1175808).

Conflict of interest statement. Neena Mitter, Bernard J. Carroll and Zhi Ping Xu have received a research grant from Nufarm LTD Australia, which involves the commercialization activities related to the BioClay. Jiaxi Yong, Miaomiao Wu, Run Zhang, Shengnan Bi and Christopher W. G. Mann declare no conflicts of interest.

References

Altpeter F, Springer NM, Bartley LE, Blechl AE, Brutnell TP, Citovsky V, Conrad LJ, Gelvin SB, Jackson DP, Kausch AP, et al. (2016) Advancing crop transformation in the era of genome editing. Plant Cell **28**: 1510–1520

Bennett M, Deikman J, Hendrix B, Iandolino A (2020) Barriers to efficient foliar uptake of dsRNA and molecular barriers to dsRNA activity in plant cells. Front Plant Sci **11**: 816

Bugatti V, Vertuccio L, Zara S, Fancello F, Scanu B, Gorrasi G (2019) Green pesticides based on cinnamate anion incorporated in layered double hydroxides and dispersed in pectin matrix. Carbohydr Polym **209**: 356–362

Cao ZB, Li B, Sun LY, Li L, Xu ZP, Gu Z (2020) 2D layered double hydroxide nanoparticles: recent progress toward preclinical/clinical nanomedicine. Small Methods **4**: 20

Chen W, Zuo H, Li B, Duan C, Rolfe B, Zhang B, Mahony TJ, Xu ZP (2018a) Clay nanoparticles elicit long-term immune responses by forming biodegradable depots for sustained antigen stimulation. Small **14**: e1704465

Chen W, Zuo H, Zhang E, Li L, Henrich-Noack P, Cooper H, Qian Y, Xu ZP (2018b) Brain targeting delivery facilitated by ligand-functionalized layered double hydroxide nanoparticles. ACS Appl Mater Interfaces **10**: 20326–20333

Cunningham FJ, Goh NS, Demirer GS, Matos JL, Landry MP (2018) Nanoparticle-mediated delivery towards advancing plant genetic engineering. Trends Biotechnol **36**: 882–897

Dalakouras A, Jarausch W, Buchholz G, Bassler A, Braun M, Manthey T, Krczal G, Wassenegger M (2018) Delivery of hairpin RNAs and small RNAs into woody and herbaceous plants by trunk injection and petiole absorption. Front Plant Sci **9**: 1253

Demirer GS, Zhang H, Goh NS, Pinals RL, Chang R, Landry MP (2020) Carbon nanocarriers deliver siRNA to intact plant cells for efficient gene knockdown. Sci Adv **6**: 12

Demirer GS, Zhang H, Matos JL, Goh NS, Cunningham FJ, Sung Y, Chang R, Aditham AJ, Chio L, Cho MJ, et al. 2019. High aspect ratio nanomaterials enable delivery of functional genetic material without DNA integration in mature plants. Nat Nanotechnol **14**: 456–464

Dietz KJ, Herth S (2011) Plant nanotoxicology. Trends Plant Sci **16**: 582–589

Giraldo JP, Landry MP, Faltermeier SM, McNicholas TP, Iverson NM, Boghossian AA, Reuel NF, Hilmer AJ, Sen F, Brew JA, et al. (2014) Plant nanobionics approach to augment photosynthesis and biochemical sensing. Nat Mater **13**: 400–408

Guo Z, Li Y, Ding SW (2019) Small RNA-based antimicrobial immunity. Nat Rev Immunol **19**: 31–44

Hoang BTL, Fletcher SJ, Brosnan CA, Ghodke AB, Manzie N, Mitter N (2022) RNAi as a foliar spray: efficiency and challenges to field applications. Int J Mol Sci **23**: 6639

Hua K, Zhang JS, Botella JR, Ma CL, Kong FJ, Liu BH, Zhu JK (2019) Perspectives on the application of genome-editing technologies in crop breeding. Mol Plant **12**: 1047–1059

Key S, Ma JKC, Drake PMW (2008) Genetically modified plants and human health. J R Soc Med **101**: 290–298

Koch A, Kogel KH (2014) New wind in the sails: improving the agronomic value of crop plants through RNAi-mediated gene silencing. Plant Biotechnol J **12**: 821–831

Kwak SY, Lew TTS, Sweeney CJ, Koman VB, Wong MH, Bohmert-Tatarev K, Snell KD, Seo JS, Chua NH, Strano MS (2019) Chloroplast-selective gene delivery and expression in planta using chitosan-complexed single-walled carbon nanotube carriers. Nat Nanotechnol **14**: 447–455

Landry MP, Mitter N (2019) How nanocarriers delivering cargos in plants can change the GMO landscape. Nat Nanotechnol **14**: 512–514

Lanz E, Gregor M, Slavík J, Kotyk A (1997) Use of FITC as a fluorescent probe for intracellular pH measurement. J Fluorescence **7**: 317–319

Lew TTS, Wong MH, Kwak SY, Sinclair R, Koman VB, Strano MS (2018) Rational design principles for the transport and subcellular distribution of nanomaterials into plant protoplasts. Small **14**: e1802086

Liu J, Nannas NJ, Fu FF, Shi J, Aspinwall B, Parrott WA, Dawe RK (2019) Genome-scale sequence disruption following biolistic transformation in rice and maize. Plant Cell **31**: 368–383

Liu P, Zhang XX, Zhang F, Xu MZ, Ye ZX, Wang K, Liu S, Han XL, Cheng Y, Zhong KL, et al. (2021) A virus-derived siRNA activates plant immunity by interfering with ROS scavenging. Mol Plant **14**: 1088–1103

Lv J, Christie P, Zhang S (2019) Uptake, translocation, and transformation of metal-based nanoparticles in plants: recent advances and methodological challenges. Environ Sci: Nano **6**: 41–59

Lv ZY, Jiang R, Chen JF, Chen WS (2020) Nanoparticle-mediated gene transformation strategies for plant genetic engineering. Plant J **104**: 880–891

Martin-Ortigosa S, Peterson DJ, Valenstein JS, Lin VS, Trewyn BG, Lyznik LA, Wang K (2014) Mesoporous silica nanoparticle-mediated intracellular cre protein delivery for maize genome editing via loxP site excision. Plant Physiol **164**: 537–547

Martiniere A, Gibrat R, Sentenac H, Dumont X, Gaillard I, Paris N (2018) Uncovering pH at both sides of the root plasma membrane interface using noninvasive imaging. Proc Natl Acad Sci USA **115**: 6488–6493

Mitter N, Worrall EA, Robinson KE, Li P, Jain RG, Taochy C, Fletcher SJ, Carroll BJ, Lu GQ, Xu ZP (2017) Clay nanosheets for topical delivery of RNAi for sustained protection against plant viruses. Nat Plants **3**: 16207

Raliya R, Saharan V, Dimkpa C, Biswas P (2018) Nanofertilizer for precision and sustainable agriculture: current state and future perspectives. J Agric Food Chem **66**: 6487–6503

Santana I, Wu H, Hu P, Giraldo JP (2020) Targeted delivery of nanomaterials with chemical cargoes in plants enabled by a biorecognition motif. Nat Commun **11**: 2045

Schwartz SH, Hendrix B, Hoffer P, Sanders RA, Zheng W (2020) Carbon dots for efficient small interfering RNA delivery and gene silencing in plants. Plant Physiol **184**: 647–657

Su Y, Ashworth V, Geitner NK, Wiesner MR, Ginnan N, Rolshausen P, Roper C, Jassby D (2020) Delivery, fate, and mobility of silver nanoparticles in citrus trees. ACS Nano **14**: 2966–2981

Su Y, Ashworth V, Kim C, Adeleye AS, Rolshausen P, Roper C, White J, Jassby D (2019) Delivery, uptake, fate, and transport of engineered nanoparticles in plants: a critical review and data analysis. Environ Sci: Nano **6**: 2311–2331

Sun B, Zhao XH, Wu YH, Cao P, Movahedi F, Liu J, Wang JJ, Xu ZP, Gu WY (2021) Mannose-functionalized biodegradable nanoparticles efficiently deliver DNA vaccine and promote anti-tumor immunity. ACS Appl Mater Interf **13**: 14015–14027

Sun D, Hussain HI, Yi Z, Siegele R, Cresswell T, Kong L, Cahill DM (2014) Uptake and cellular distribution, in four plant species, of fluorescently labeled mesoporous silica nanoparticles. Plant Cell Rep **33**: 1389–402

Torti S, Schlesier R, Thümmler A, Bartels D, Römer P, Koch B, Werner S, Panwar V, Kanyuka K, Wirén NV, Jones JDG, Hause G, Giritch A, Gleba Y (2021) Transient reprogramming of crop plants for agronomic performance. Nat Plants **7**: 159–171

Uslu VV, Dalakouras A, Steffens VA, Krczal G, Wassenegger M (2022) High-pressure sprayed siRNAs influence the efficiency but not the profile of transitive silencing. Plant J **109**: 1199–1212

Wang JW, Grandio EG, Newkirk GM, Demirer GS, Butrus S, Giraldo JP, Landry MP (2019) Nanoparticle-mediated genetic engineering of plants. Mol Plant **12**: 1037–1040

Wu YH, Gu WY, Chen C, Do ST, Xu ZP (2018) Optimization of formulations consisting of layered double hydroxide nanoparticles and small interfering RNA for efficient knockdown of the target gene. ACS Omega **3**: 4871–4877

Xu ZP, Stevenson GS, Lu CQ, Lu GQM, Bartlett PF, Gray PP (2006a) Stable suspension of layered double hydroxide nanoparticles in aqueous solution. J Am Chem Soc **128**: 36–37

Xu ZP, Walker TL, Liu KL, Cooper HM, Lu GQM, Bartlett PF (2007) Layered double hydroxide nanoparticles as cellular delivery vectors of supercoiled plasmid DNA. Int J Nanomed **2**: 163–174

Xu ZP, Zeng HC (2001) Abrupt structural transformation in hydrotalcite-like compounds Mg1-xAlx(OH)(2)(NO3)(x)center dot nH(2)O as a continuous function of nitrate anions. J Phys Chem B **105**: 1743–1749

Xu ZP, Zeng QH, Lu GQ, Yu AB (2006b) Inorganic nanoparticles as carriers for efficient cellular delivery. Chem Eng Sci **61**: 1027–1040

Yong J, Zhang R, Bi S, Li P, Sun L, Mitter N, Carroll BJ, Xu ZP (2021) Sheet-like clay nanoparticles deliver RNA into developing pollen to efficiently silence a target gene. Plant Physiol **187**: 886–899

Zhang H, Cao Y, Xu D, Goh NS, Demirer GS, Cestellos-Blanco S, Chen Y, Landry MP, Yang P (2021) Gold-nanocluster-mediated delivery of siRNA to intact plant cells for efficient gene knockdown. Nano Lett **21**: 5859–5866

Zhang H, Demirer GS, Zhang H, Ye T, Goh NS, Aditham AJ, Cunningham FJ, Fan C, Landry MP (2019) DNA nanostructures coordinate gene silencing in mature plants. Proc Natl Acad Sci USA **116**: 7543–7548

Zhao L, Lu L, Wang A, Zhang H, Huang M, Wu H, Xing B, Wang Z, Ji R (2020) Nano-biotechnology in agriculture: use of nanomaterials to promote plant growth and stress tolerance. J Agric Food Chem **68**: 1935–1947

Zhao ZG, Shen T, Xu HJ (1989) The absorption and structure of fluorescein and its ethyl derivatives in various solutions. Spectrochim Acta Part A **45**: 1113–1116